

# *c-a-ca* Mean Field RVB Model of CuNCN Physics. Structure Manifestations of the RVB Transitions.

April 4, 2021

April 4, 2021

A.L. Tchougréeff<sup>a,b</sup> and R. Dronskowski<sup>a</sup>

<sup>a</sup>Institut für anorganische Chemie RWTH-Aachen University, Landoltweg  
1, D-52056, Aachen, Germany;

<sup>b</sup>Poncelet Lab., Independent University of Moscow, Moscow Center for  
Continuous Mathematical Education, Moscow, Russia

## Abstract

We propose a new form of the frustrated Heisenberg antiferromagnetic Hamiltonian with spatially anisotropic exchange parameters  $J_c$ ,  $J_a$ , and  $J_{ac}$  extended along the  $c$ ,  $a$ , and  $a \pm c$  lattice directions and apply it to describe fascinating physics of copper carbodiimide CuNCN in the assumption of resonating valence bond (RVB) type of its phases. These are invoked to explain the intriguing absence of magnetic order in CuNCN down to 4 K. We show that the quasiparticle spectrum of the RVB model of the proposed Hamiltonian has three principal regimes: (i) one with two pairs of lines of nodes, (ii) one with a pair of lines of nodes (termed as 1D- and Q1D-RVB states), (iii) and one with two pseudogaps and four nodal points (2D-RVB). We present a complete parameters-temperature phase diagram of the *c-a-ca*-RVB model constructed with use of the high-temperature expansion of the free energy. The phase diagram thus obtained contains eight different phases whose magnetic behavior includes Curie and Pauli paramagnetism (respectively, in disordered and 1D- or Q1D-RVB phases), and

gapped (quasi-Arrhenius) paramagnetism (2D-RVB phases). Adding magnetostriction and elastic terms to the free energy of the model we derive possible structural manifestations of transitions between various RVB phases of the *c-a-ca*-model of CuNCN. Assuming a sequence of transitions between RVB phases to occur in CuNCN while temperature decreases explains the features observed in the temperature runs of the magnetic susceptibility and lattice constants. Confronting these with the magnetic susceptibility and structure data measured as functions of temperature in the range between *ca.* 20 and 200 K we show a remarkably good agreement between our theoretical predictions and the experiment as reached by ascribing the model parameters values which are intuitively acceptable both in terms of their absolute and relative magnitudes and of the character of their geometry dependence.

# Contents

<b>1</b>	<b>Introduction</b>	<b>4</b>
<b>2</b>	<b>RVB mean-field analysis of the model</b>	<b>6</b>
2.1	Quasiparticle spectrum . . . . .	6
2.2	Free energy and phases of the model . . . . .	10
<b>3</b>	<b>Physical properties within the model</b>	<b>15</b>
3.1	Magnetic susceptibility . . . . .	15
3.2	Structure manifestations of transitions between RVB phases .	17
3.2.1	Theory . . . . .	17
3.2.2	Synchrotron measurements on CuNCN as explained by RVB phase transitions . . . . .	18
<b>4</b>	<b>Conclusion</b>	<b>26</b>
<b>A</b>	<b>Equations of motion and self consistency equations.</b>	<b>30</b>
<b>B</b>	<b>High-temperature expansion.</b>	<b>32</b>
<b>C</b>	<b>Quasiparticle densities of states in various RVB phases</b>	<b>32</b>
<b>D</b>	<b>Theory of the structural manifestations of the RVB states.</b>	<b>34</b>
<b>E</b>	<b>Estimate of the force matrix from the elastic constants</b>	<b>36</b>

# 1 Introduction

Recently CuNCN phase had been obtained and a series of measurements had been performed of its spatial structure and magnetic susceptibility, electric resistivity, heat capacity (all *vs. T*) [1]. Although on the basis of analogy with other materials of the MNCN series ( $M = \text{Mn, Fe, Co, Ni}$ ) one would expect more or less standard antiferromagnetic behavior, it turned out that at low temperature this material does not manifest any magnetic neutron scattering [2]. The plausible explanation of the latter fact as "absence of local momenta" may be, however, misleading since the absence of the magnetic scattering means only the absence of the long range magnetic order (LRMO) (evanescence of the spin-spin correlation function), not the absence of the local momenta themselves. Similar situation can be observed in the crystals of Cu-carboxylate dimers where local spins 1/2 do present on each  $\text{Cu}^{2+}$  ion, but form isolated singlet pairs so that no long range magnetic order does exist. On the structural grounds one cannot expect anything like this in CuNCN since among the contacts of individual  $\text{Cu}^{2+}$  ions one cannot select any which would be uniquely strong. This brought us [3, 4, 5, 6] to the idea that the ground state of this material may be related to the RVB state of the  $\text{Cu}^{2+}$  local spins 1/2.

Previously we assumed [3, 4, 5, 6] that from the materials structure Fig. 1 [1] one can conjecture an anisotropic triangular antiferromagnetic Heisenberg model with the plane corresponding to the  $ab$  plane of the structure. This was not easy to reconcile with the intuitive picture [7] of the most important couplings to be extended in the  $a$  and  $c$  directions. This brings us to the idea to consider more antiferromagnetic couplings. This results in the Heisenberg model with the Hamiltonian:

$$\sum_{\mathbf{r}} \sum_{\tau} J_{\tau} \mathbf{S}_{\mathbf{r}} \mathbf{S}_{\mathbf{r}+\tau} \quad (1)$$

where the translation vector  $\tau$  takes four values  $\tau_i; i = 1 \div 4; \tau_1 = (a, 0); \tau_2 = (0, c); \tau_3 = (a, c); \tau_4 = (a, -c)$  with the interaction of the strength  $J_a$  along the lattice vector  $\tau_1$  (two neighbors), with a strength  $J_c$  along the lattice vector  $\tau_2$  (two neighbors as well), and interaction of the strength  $J_{ac}$  along the lattice vectors  $\tau_3$  and  $\tau_4$  (two neighbors along each). The importance of the diagonal  $J_{ac}$  couplings in the  $\tau_3$  and  $\tau_4$  directions have been recently reiterated in [8] although it is fairly in a line with the standard considerations of [7]. Either interactions along  $\tau_1$  and  $\tau_2$  or those along  $\tau_3$  and  $\tau_4$  taken

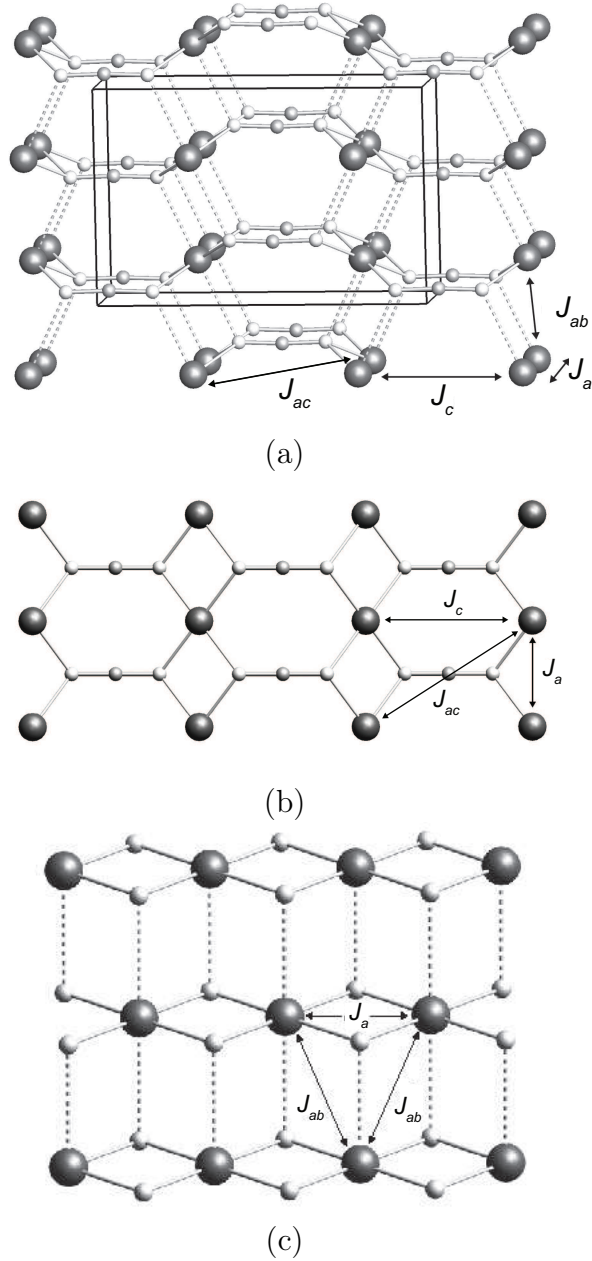


Figure 1: The CuNCN crystal structure and the exchange parameters included in the consideration. (a) shows the overall view on the structure. A stronger  $J_c$  extends in the  $c$  direction; somewhat weaker  $J_a$  extends in the  $a$ -direction. The weakest  $J_{ab}$  extends along the  $b \pm a$  directions. (b) shows the  $ac$  planes of CuNCN. The interactions in all cases are mediated by the  $\text{NCN}^{2-}$  moieties. Two stronger interactions ( $J_c$  and  $J_{ac}$ ) are mediated by the  $\pi$ -system of  $\text{NCN}^{2-}$ ; somewhat weaker  $J_a$  is strongly contributed by a ferromagnetic cointerpoise terms dependent on the hybridization at the N atoms. (c) shows for completeness the  $ab$  planes of the CuNCN which are not considered in the present paper.

separately must lead to an antiferromagnetic state. However, when considered simultaneously they interfere leading to a frustration not allowing the spins to arrange in any LRMO state. For similar systems a variety of RVB states have been proposed [9, 10]. Ground state of a similar, but spatially isotropic  $J_1 J_2 J_3$  model have been treated recently by various methods and it has been shown that spin-liquid states are very probable [11]. In the present paper we consider in details the RVB states of the above model in the RVB mean-field approximation and apply this to analysis of the experimental data so far obtained for CuNCN.

## 2 RVB mean-field analysis of the model

### 2.1 Quasiparticle spectrum

Following the method [12] used by us previously [3, 5, 6] we base the analysis of the Hamiltonian eq. (1) on getting back to the fermion (spinon) representation by the standard move:

$$\mathbf{S}_i = \frac{1}{2} c_{i\alpha}^+ \boldsymbol{\sigma}_{\alpha\beta} c_{i\beta}, \quad (2)$$

where  $c_{i\sigma}^+$  ( $c_{i\sigma}$ ) are the fermion creation (annihilation) operators;  $\boldsymbol{\sigma}_{\alpha\beta}$  are the elements Pauli matrices and the summation over repeating indices is assumed. Applying standard technique as described in Appendix A we reduce the problem to the set of  $2 \times 2$  eigenvalue problems for each wave vector  $\mathbf{k}$ :

$$\begin{pmatrix} \xi_{\mathbf{k}} & \Delta_{\mathbf{k}} \\ \Delta_{\mathbf{k}}^* & -\xi_{\mathbf{k}} \end{pmatrix} \begin{pmatrix} u_{\mathbf{k}} \\ v_{\mathbf{k}} \end{pmatrix} = E_{\mathbf{k}} \begin{pmatrix} u_{\mathbf{k}} \\ v_{\mathbf{k}} \end{pmatrix}$$

with

$$\begin{aligned} \xi_{\mathbf{k}} &= -3 \sum_{\tau} J_{\tau} \xi_{\tau} \cos(\mathbf{k}\tau) \\ \Delta_{\mathbf{k}} &= 3 \sum_{\tau} J_{\tau} \Delta_{\tau} \cos(\mathbf{k}\tau) \end{aligned}$$

(summation over  $\tau$  extends to  $\tau_i; i = 1 \div 4$ ) which results in the excitation spectrum of the form:

$$E_{\mathbf{k}} = \pm \sqrt{\xi_{\mathbf{k}}^2 + |\Delta_{\mathbf{k}}|^2}$$

whose eigenvectors are combinations of the destruction and creation operators with the above Bogoliubov transformation coefficients. The above set of equations closes by the selfconsistency conditions of the form:

$$\begin{aligned}\xi_\tau &= -\frac{1}{2N} \sum_{\mathbf{k}} \exp(i\mathbf{k}\tau) \frac{\xi_{\mathbf{k}}}{E_{\mathbf{k}}} \tanh\left(\frac{E_{\mathbf{k}}}{2\theta}\right) \\ \Delta_\tau &= \frac{1}{2N} \sum_{\mathbf{k}} \exp(-i\mathbf{k}\tau) \frac{\Delta_{\mathbf{k}}}{E_{\mathbf{k}}} \tanh\left(\frac{E_{\mathbf{k}}}{2\theta}\right)\end{aligned}\quad (3)$$

for the order parameters (OPs)  $\xi_\tau, \Delta_\tau$ . The lattice symmetry considerations allow us to restrict ourselves by six OPs:  $\xi_a, \xi_c, \xi_{ac}; \Delta_a, \Delta_c, \Delta_{ac}$ . Using the standard moves foreseen for the  $SU(2)$  symmetric solutions as described in Appendix A we arrive to the quasiparticle spectrum:

$$E_{\mathbf{k}}^2 = 9 \left( J_a^2 \zeta_a^2 \cos^2 x + J_c^2 \zeta_c^2 \cos^2 z + 4J_{ac}^2 \zeta_{ac}^2 \cos^2 x \cos^2 z \right), \quad (4)$$

where we set  $x = \mathbf{k}_x; z = \mathbf{k}_z$  and introduced effective OPs  $\zeta_a = \sqrt{\xi_a^2 + \eta_a^2}$ ,  $\zeta_c = \sqrt{\xi_c^2 + \eta_c^2}$ , and  $\zeta_{ac} = \sqrt{\xi_{ac}^2 + \eta_{ac}^2}$ .

The spectrum eq. (4) is depicted in Fig. 2.

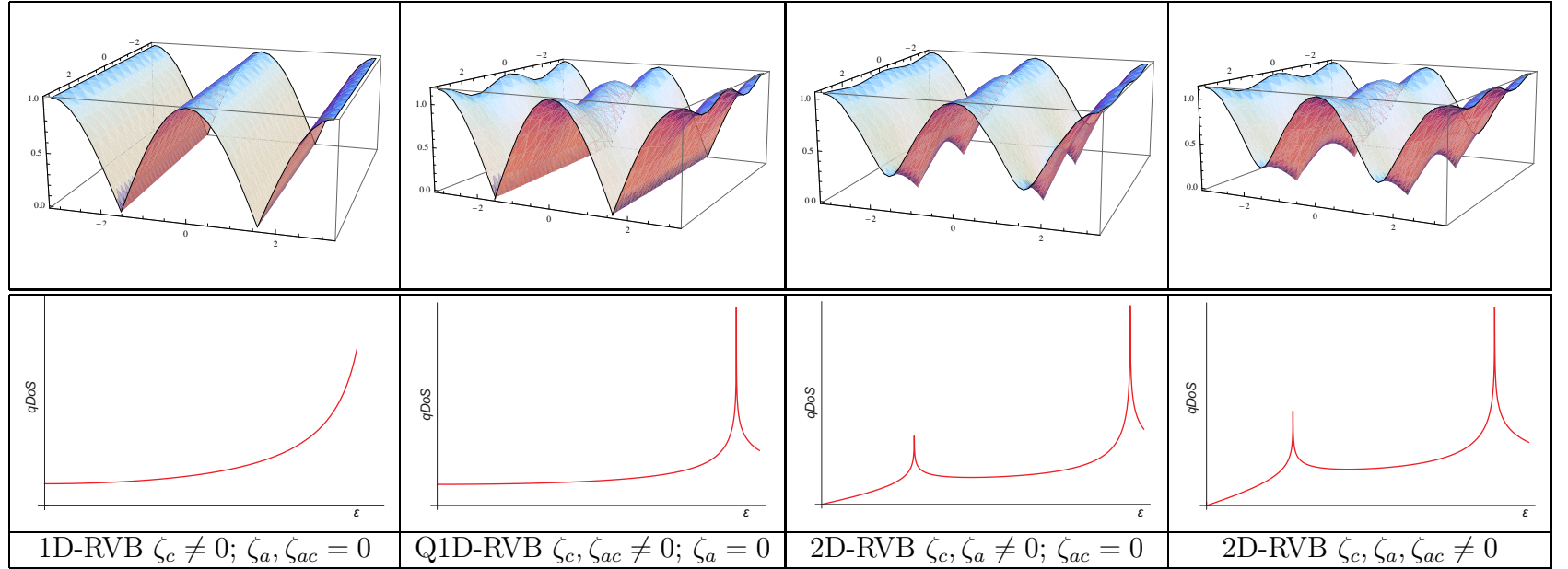


Figure 2: Dispersion laws of the  $c$ - $a$ - $ca$ -RVB model for several exemplary values of the pseudogap/bandwidth parameters  $A = 3J_a\zeta_a$ ;  $C = 3J_c\zeta_c$ ;  $B = 3J_{ac}\zeta_{ac}$  indicating characteristic feature of the quasiparticle spectrum in different RVB states and the sketches of the relevant qDoS (see text for the details).



If either of the OPs  $\zeta_a$  or  $\zeta_c$  is the only nonvanishing OP, the quasiparticle spectrum acquires corresponding lines of nodes  $z = \pm\frac{\pi}{2}$  or respectively  $x = \pm\frac{\pi}{2}$  where the quasiparticles have zero energy. Since the dispersion of quasiparticles takes place in only one crystallographic direction ( $a$  or  $c$ ) we spell these states as one-dimensional (1D-RVB) states. In the low energy range the quasiparticle density of states (qDoS) in the 1D-RVB states is constant. Due to the dispersionless ridge in the spectrum the qDoS diverges at the ceiling of the quasiparticle band [3]. This type of behavior is similar to that of the spinons of the anisotropic triangular Heisenberg model as found in [13] and considered in our previous work [3, 4, 5, 6] in relation to CuNCN. If both OPs  $\zeta_{a,c}$  vanish and the OP  $\zeta_{ac}$  does not two pairs of nodal lines exist along which the quasiparticles have zero energy. In this state the qDoS diverges logarithmically at zero energy. We, however, do not focus on this peculiar state and it is not shown in Fig. 2.

If either of the nonvanishing OPs  $\zeta_{a,c}$  is complemented by the nonvanishing OP  $\zeta_{ac}$  quasi-1D-RVB (Q1D-RVB) states appear. The difference with the true 1D-RVB states is that in the Q1D-RVB states there exists a nonvanishing dispersion in the direction transversal to the node lines. At the higher energies the quasiparticle spectrum of these states has maxima and saddle points instead of the ridge. Thus the qDoS develops a finite hop at the ceiling of the quasiparticle band and a van Hove singularity at somewhat lower energy, which serves as a pseudogap. By contrast, if the nonvanishing OP's are  $\zeta_c$  and  $\zeta_a$  then irrespective to the value of the OP  $\zeta_{ac}$  there are no lines of nodes, but four nodal points ( $\mathbf{k} = (\pm\frac{\pi}{2}, \pm\frac{\pi}{2})$ ) of vanishing quasiparticle energies. In the vicinity of these points the quasiparticles are massless as in the disordered (pseudometallic) phase of the graphite monolayers [14]. The two possible states of this type are spelled as 2D-RVB ones. The qDoS in 2D-RVB states vanishes at the zero energy, being proportional to the energy well below the smaller pseudogap. Otherwise the quasiparticle dispersion law has saddle points at the two pseudogap energies and thus the qDoS of 2D-RVB state develops two van Hove singularities at the corresponding pseudogaps.

## 2.2 Free energy and phases of the model

Following Ref. [10] one can write immediately the free energy of the *c-a-ca* model in terms of the above OPs:

$$F = 3J_a\zeta_a^2 + 3J_c\zeta_c^2 + 6J_{ac}\zeta_{ac}^2 - \frac{2\theta}{4\pi^2} \int_{BZ} \ln \left( 2 \cosh \left( \frac{E_{\mathbf{k}}}{2\theta} \right) \right) d^2\mathbf{k}. \quad (5)$$

where  $\theta = k_B T$  (BZ stands for the integration over the Brillouin zone). Minima of eq. (5) with respect to  $\zeta$ 's correspond to various possible phases of the system. We postpone the study of the ground state (zero temperature limit) of the present model to further publications and focus on the results which can be obtained with use of the high temperature expansion (technicalities are explained in Appendix B).

The results obtained by minimizing the high temperature expansion of eq. (5) with respect to the OPs are depicted in the parameter phase diagram Fig. 3 and present in Table 1. Fig. 3 represents the phase diagram for the triple of exchange parameters subject to the condition  $J_a + J_c + J_{ac} = 1$  and a series of temperatures between 0.4 and 0.01 (the fractions of the above sum of the exchange parameters is meant). One can see that eight phases are possible. For the temperature above either of three critical ones:

$$\theta_{\tau}^{\text{crit}} = \frac{3}{8} J_{\tau}. \quad (6)$$

the Curie paramagnetic phase: (1 - grey) in which all three OP's equal to zero persists. Below these temperatures gapless phases appear in respective corners of the parameter phase diagram. Their spectra are however quite different. There are two 1D-RVB phases with OPs  $\zeta_c$  or  $\zeta_a \neq 0$  (2 - red and 3 - green areas in Fig. 3). Due to the constant qDoS at the zero energy they have to exhibit a temperature independent paramagnetism which could be termed as Pauli paramagnetism had it been due to conductivity electrons. Thus we spell it as a quasi-Pauli one. The paramagnetic phase with  $\zeta_{ac} \neq 0$  (4 - blue area in Fig. 3) is quite different: the maximum of the spectrum at the ceiling of the quasiparticle band assures a constant value of the density of states (a finite hop) rather a divergence as in 1D-RVB states, and logarithmically diverges at the zero energy. Thus one has to expect the paramagnetic susceptibility to logarithmically diverge at zero temperature in this phase.

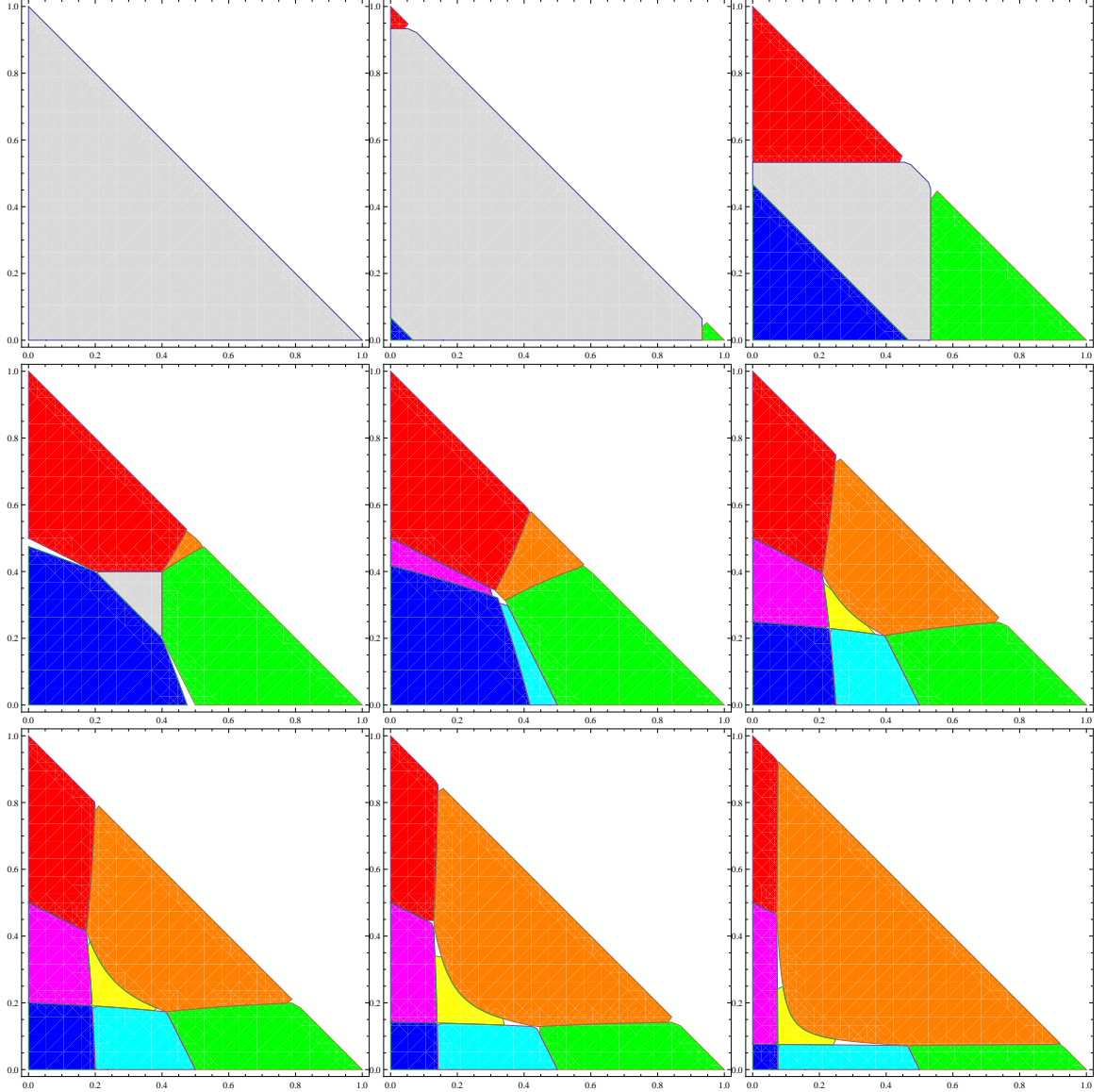


Figure 3: Parameter phase diagrams for the  $c$ - $a$ - $ca$ -RVB model in the high-temperature approximation. The abscissa and ordinate represent respectively  $J_a$  and  $J_c$ ; the entire parameters set is subject to the condition  $J_a + J_c + J_{ac} = 1$ . The temperatures as fractions of  $J_a + J_c + J_{ac}$  from the left upper diagram to the right lower one are 0.4, 0.35, 0.2, 0.15, 0.1, 0.04, 0.03, 0.02, 0.01 (follow rows). The colour coding for phases is: Curie paramagnetic, all OPs are zero - gray, only one nonvanishing OP: red, green (1D-RVB, Pauli paramagnet), blue for  $\zeta_c, \zeta_a, \zeta_{ac} \neq 0$ , respectively; one OP vanishing: magneta, cyan (Q1D-RVB, Pauli paramagnet), orange for  $\zeta_a$ , or  $\zeta_c$ , or  $\zeta_{ac} = 0$ , respectively - observe the order of the list; yellow codes the phase with three nonvanishing OPs. Orange and yellow phases (2D-RVB) feature combination of the gapped Arrhenius-like temperature dependence of magnetic susceptibility and its linear dependence well below the pseudogap.

Below critical temperatures:

$$\theta_{\tau \rightarrow \tau, \tau'}^{\text{crit}} = \frac{J_{\tau'}}{8} \left( 1 - \frac{2J_{\tau'}}{3J_{\tau}} \right)^{-1} = \frac{3J_{\tau}J_{\tau'}}{8(3J_{\tau} - 2J_{\tau'})} \quad (7)$$

whose expression is already familiar from the high-temperature mean field analysis [3, 4] of the RVB states in the triangular anisotropic Heisenberg model, respective phases with two nonvanishing OP's  $\zeta_{\tau}$  and  $\zeta_{\tau'}$  appear (the notation refers to transition from the state where only one OP  $\zeta_{\tau} \neq 0$  to a state where two OP's  $\zeta_{\tau}, \zeta_{\tau'} \neq 0$ ). The phases with two nonvanishing OPs as well are different. If one of the nonvanishing OPs is  $\zeta_{ac}$  (5 - magenta and 6 - cyan areas in Fig. 3) the qDoS is constant at the zero energy and thus quasi-Pauli paramagnetism has to be expected in these Q1D-RVB phases.

The phase with three nonvanishing OP's (8 - yellow) is a transient one. It first appears below the *octal* point  $J_a = J_{ac} = J_c = \frac{1}{3}; \theta^* = 1/8$  where the Curie paramagnetic phase (grey) completely disappears and shows up from the above Q1D-RVB phases (magenta or cyan) at the critical temperatures

$$\theta_{\tau, ac \rightarrow a, c, ac}^{\text{crit}} = \frac{3J_{ac}J_{\bar{\tau}}}{8(3J_{ac} - 2J_{\bar{\tau}})}, \quad (8)$$

( $\bar{\tau} = c, a$  for  $\tau = a, c$ ) but exists *above* the critical temperature of:

$$\theta_{a, c, ac}^{\text{crit}} = \frac{3J_a J_{ac} J_c}{8(3J_a J_{ac} - 5J_a J_c + 3J_{ac} J_c)} \quad (9)$$

where it switches to the 2D-RVB phase with only two nonvanishing OP's  $\zeta_c$  and  $\zeta_a$  (7 - orange). That latter phase appears also from the 1D-RVB phases (red and green) at the critical temperatures given by eq. (7). The only difference between the dispersion laws of these two phases as depicted in 3-rd and 4-th columns of Fig. 2 is somewhat more pronounced dispersion along a "ridge" in the case of the phase with three nonvanishing OPs. Otherwise both 2D-RVB phases have a qDoS with two van-Hove singularities at the energies of their characteristic pseudogaps and the physics of these latter two phases has to be pretty similar. It can be checked that the transitions are largely of the second order, that is to say that the OPs split from zero continuously at the corresponding transition temperatures. The interphase borders between the 1D-RVB and Q1D-RVB phases (2/5 and 3/6 or red/magenta and green/cyan, respectively) are special. Phases 2 and 3 are unstable towards developing the nonvanishing OP  $\zeta_{ac}$  when the exchange

parameter  $J_{ac}$  turns to be larger than, respectively, the exchange parameters  $J_c$  or  $J_a$  at whatever temperature. On the lines  $J_{ac} = J_c$  or  $J_{ac} = J_a$  where the OP  $\zeta_{ac}$  bounces from zero the transition temperatures from the Curie paramagnetic state (phase 1 - grey) to either 1D-RVB or Q1D-RVB Pauli paramagnetic phases pairwise coincide (that is to 2 and 5 *i.e.* to red and magenta or to 3 and 6 *i.e.* to green and cyan). That means that if the system parameters fall in the corresponding (magenta or cyan) areas and it is cooled below the critical temperature eq. (7) with  $\tau = ac, \tau' = a, c$ , it directly goes from the Curie paramagnetic phase to the corresponding Q1D-RVB phase, rather to a 1D-RVB phase.

In the last column of Table 1 we show the analytical forms of the qDoS characteristic for the respective specific forms of the quasiparticle spectrum. It turned out quite unexpectedly, that these qDoS can be found analytically for all phases of the *c-a-ca* RVB-model. Leaving the details of the derivation for further publications we provide a sketch of the derivation in Appendix C.

Table 1: Temperature dependencies of the OPs for possible phases of the  $c$ - $a$ - $ca$ -RVB model in the high-temperature approximation. The areas of the existence of the corresponding phases are those where the expressions under the square roots are positive. The last column gives the qDoS in the respective phases. There  $K$  stands for the complete elliptic integral of the first kind. Details of derivation will be communicated elsewhere. Their characteristic graphs are given in Fig. 2.

	No	Color code	OP's <i>vs.</i> $\theta$	$g(\varepsilon)$
Curie	1	Gray	$\zeta_c = \zeta_a = \zeta_{ac} = 0$	$\delta(\varepsilon)$
Pauli	2	Red	$\zeta_a = \zeta_{ac} = 0; \zeta_c = \frac{4\theta}{3J_c} \sqrt{1 - 8\theta/3J_c}$	$\frac{2}{\pi} \frac{1}{\sqrt{C^2 - \varepsilon^2}}$
Pauli	3	Green	$\zeta_c = \zeta_{ac} = 0; \zeta_a = \frac{4\theta}{3J_a} \sqrt{1 - 8\theta/3J_a}$	$\frac{2}{\pi} \frac{1}{\sqrt{A^2 - \varepsilon^2}}$
$\frac{2\mu_B^2}{\pi^2 B} \ln \frac{32B}{\pi e^{\gamma\theta}}$	4	Blue	$\zeta_c = \zeta_a = 0; \zeta_{ac} = \frac{4\theta}{3J_{ac}} \sqrt{1 - 8\theta/3J_{ac}}$	$\frac{2}{\pi^2 B} K\left(\frac{\sqrt{4B^2 - \varepsilon^2}}{2B}\right)$
Pauli	5	Magenta	$\begin{cases} \zeta_a = 0 \\ \zeta_c = \frac{4\theta\sqrt{3J_{ac}J_c - 24\theta J_{ac} + 16\theta J_c}}{3\sqrt{3}J_c\sqrt{J_c J_{ac}}} \\ \zeta_{ac} = \frac{8}{3}\sqrt{\frac{2}{3}}\frac{\theta}{J_{ac}}\sqrt{\frac{\theta(J_{ac} - J_c)}{J_{ac}J_c}} \end{cases}$	$\frac{4}{\pi^2} \frac{K\left(\frac{2B}{\sqrt{4B^2 + C^2 - \varepsilon^2}}\right)}{\sqrt{4B^2 + C^2 - \varepsilon^2}}$
Pauli	6	Cyan	$\begin{cases} \zeta_a = \frac{4\theta\sqrt{3J_{ac}J_a - 24\theta J_{ac} + 16\theta J_a}}{3\sqrt{3}J_a\sqrt{J_a J_{ac}}} \\ \zeta_c = 0 \\ \zeta_{ac} = \frac{8}{3}\sqrt{\frac{2}{3}}\frac{\theta}{J_{ac}}\sqrt{\frac{\theta(J_{ac} - J_a)}{J_{ac}J_a}} \end{cases}$	$\frac{4}{\pi^2} \frac{K\left(\frac{2B}{\sqrt{4B^2 + A^2 - \varepsilon^2}}\right)}{\sqrt{4B^2 + A^2 - \varepsilon^2}}$
Arrhenius	7	Orange	$\begin{cases} \zeta_a = \frac{4\theta\sqrt{3J_aJ_c - 24\theta J_c + 16\theta J_a}}{3\sqrt{5}J_a\sqrt{J_a J_c}} \\ \zeta_c = \frac{4\theta\sqrt{3J_aJ_c - 24\theta J_a + 16\theta J_c}}{3\sqrt{5}J_c\sqrt{J_a J_c}} \\ \zeta_{ac} = 0 \end{cases}$	$\begin{cases} \frac{4\varepsilon}{\pi^2 AC} K\left(\frac{\varepsilon\sqrt{A^2 + C^2 - \varepsilon^2}}{AC}\right), \varepsilon < \min(A, C) \\ \frac{4}{\pi^2} \frac{K\left(\frac{AC}{\varepsilon\sqrt{A^2 + C^2 - \varepsilon^2}}\right)}{\sqrt{A^2 + C^2 - \varepsilon^2}}, \min(A, C) < \varepsilon < \max(A, C) \\ \frac{4\varepsilon}{\pi^2 AC} K\left(\frac{\varepsilon\sqrt{A^2 + C^2 - \varepsilon^2}}{AC}\right), \varepsilon > \max(A, C) \end{cases}$
Arrhenius	8	Yellow	$\begin{cases} \zeta_a = \frac{4\theta\sqrt{3J_aJ_{ac} - 24\theta J_{ac} + 16\theta J_a}}{3\sqrt{3}J_a\sqrt{J_a J_{ac}}} \\ \zeta_c = \frac{4\theta\sqrt{3J_cJ_{ac} - 24\theta J_{ac} + 16\theta J_c}}{3\sqrt{3}J_c\sqrt{J_c J_{ac}}} \\ \zeta_{ac} = \frac{4\theta\sqrt{24\theta J_{ac}J_a - 40\theta J_aJ_c + 24\theta J_{ac}J_c - 3J_aJ_{ac}J_c}}{9J_{ac}\sqrt{J_aJ_cJ_{ac}}} \end{cases}$	$\begin{cases} \frac{4}{\pi^2} \frac{\varepsilon K\left(\sqrt{\frac{\varepsilon^2(A^2 + 4B^2 + C^2 - \varepsilon^2)}{A^2C^2 + 4B^2\varepsilon^2}}\right)}{\sqrt{A^2C^2 + 4B^2\varepsilon^2}}, \varepsilon < \min(A, C) \\ \frac{4}{\pi^2} \frac{K\left(\sqrt{\frac{A^2C^2 + 4B^2\varepsilon^2}{\varepsilon^2(A^2 + 4B^2 + C^2 - \varepsilon^2)}}\right)}{\sqrt{A^2 + 4B^2 + C^2 - \varepsilon^2}}, \min(A, C) < \varepsilon < \max(A, C) \\ \frac{4}{\pi^2} \frac{\varepsilon K\left(\sqrt{\frac{\varepsilon^2(A^2 + 4B^2 + C^2 - \varepsilon^2)}{A^2C^2 + 4B^2\varepsilon^2}}\right)}{\sqrt{A^2C^2 + 4B^2\varepsilon^2}}, \varepsilon > \max(A, C) \end{cases}$

## 3 Physical properties within the model

### 3.1 Magnetic susceptibility

We use the standard definition of the magnetic susceptibility per spin:

$$\chi = -2\mu_B^2 \int g(\varepsilon) \frac{\partial f(\frac{\varepsilon}{T})}{\partial \varepsilon} d\varepsilon \quad (10)$$

where  $f(\dots)$  is the Fermi distribution function. The qualitative behavior of the susceptibility as derived from the characteristic features of the qDoS is designated in the first column of Table 1. It is not surprising that the temperature independent paramagnetism (conditionally denoted as “Pauli”, although it goes about some other quasiparticles rather the band electrons in metals) takes place in the phases (Nos 2, 3, 5, and 6) with a constant density of states at the zero energy. The gapless phase 4 with two pairs of intersecting node lines manifests a logarithmic singularity in the qDoS at the Fermi level. This singularity, however, integrates and produces a logarithmic divergence of the susceptibility at the zero temperature. For two phases (Nos 7 and 8) with nodal points in the dispersion law and linear dependence of the qDoS in the low-energy range one has to expect as well a linear dependence of the susceptibility on temperature in the low-temperature region (well below the lower pseudogap) superimposed with a quasi-Arrhenius behavior with characteristic energy of the pseudogap at higher temperature. That rich variety of possible phases on the *c-a-ca*-RVB model allows to eventually explain the magnetic behavior of CuNCN.

As we mentioned above and previously [3, 4, 5] the absence of magnetic scattering in CuNCN is perfectly explained by the hypothesis of the RVB character of its phases. The temperature independent paramagnetism of CuNCN as observed at higher temperatures is explained by formation of one of many 1D- or Q1D-RVB phases (Nos 2, 3, 5, and 6). That means that only one of the OPs  $\zeta_a$  or  $\zeta_c$  is nonvanishing. As previously we assume that this phase sets on at some pretty high temperature which cannot be directly checked due to decomposition of the material [4]. For a pseudogap to open in a (Q)1D-RVB state with, say, nonvanishing  $\zeta_c$  (phase 2, red or phase 5, magenta) one needs that at an observable critical temperature the OP  $\zeta_a$  splits from zero (phase 7, orange or phase 8, yellow) since for the pseudogap to open it cannot be the  $\zeta_{ac}$  OP. Thus we assume the following form for the

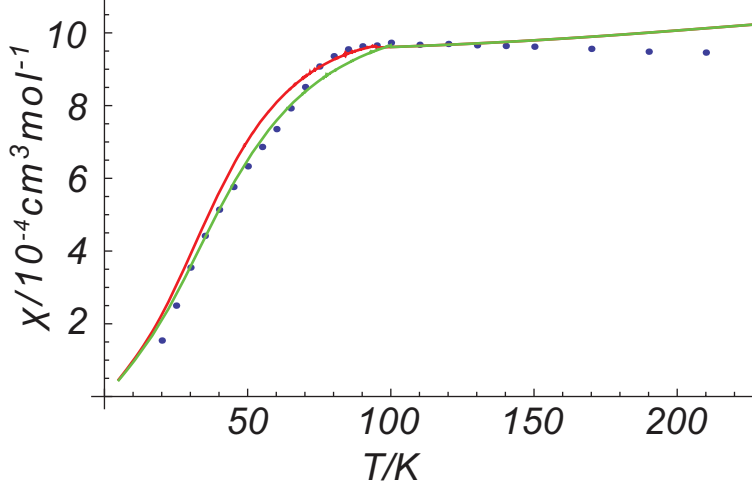


Figure 4: EPR magnetic susceptibility of CuNCN Ref. [4] (blue dots) as compared with the results of numerical integration with the qDoS for the phase 7. One can easily see the linear tail in the low temperature range with no experimental points. Otherwise the parameters are  $\theta^{\text{crit}} = 95$  K,  $\nu = 0.6$ ,  $A_0 = 145$  K,  $C = 1250$  K (red line) and  $\theta^{\text{crit}} = 100$  K,  $\nu = 0.5$ ,  $A_0 = 150$  K,  $C = 1250$  K (green line).

temperature dependence of the pseudogap  $A$ :

$$A(\theta) = A_0 \left(1 - \frac{\theta}{\theta^{\text{crit}}}\right)^\nu \quad (11)$$

below the critical temperature  $\theta^{\text{crit}}$  (where by  $\theta^{\text{crit}}$  one of the temperatures  $\theta_{c \rightarrow c, a}^{\text{crit}}$  or  $\theta_{c, ac \rightarrow c, a, ac}^{\text{crit}}$  is meant) and perform the numerical integration of eq. (10) for the susceptibility with the qDoS for the RVB phase with two pseudogaps where we also set  $B = 0$ .<sup>1</sup>

We performed several attempts and concluded that the values of  $\theta^{\text{crit}}$  ( $\theta_{c \rightarrow c, a}^{\text{crit}}$  or  $\theta_{c, ac \rightarrow c, a, ac}^{\text{crit}}$ ),  $A_0$ ,  $C$ , and  $\nu$  can be adjusted to reproduce the experimental run of the susceptibility [4]. The results are shown in Fig. 4. The

<sup>1</sup>We notice that due to the character of the dependence of the OP  $\zeta_{ac}$  on the model parameters shown in Table 1 and the plausible assumption of the relation  $J_{ac} \gtrsim J_c$  between the exchange parameter, which needs to hold for the Q1D-RVB phase (magenta) to appear, this OP can never be large. Thus the characteristics of the system are basically not affected by the specific value of the  $J_{ac}$  since its contribution is scaled down by the small value of  $\zeta_{ac}$ .



value of  $C$  is rather stable. Its scale is given by the magnitude of the Pauli paramagnetic susceptibility at a higher temperature and can be used to fit the parameters of the original model eq. (1). The sets of parameters  $\theta^{\text{crit}} = 80$  K,  $\nu = 0.75$ ,  $A_0 = 240$  K or  $\theta^{\text{crit}} = 100$  K,  $\nu = 0.5$ ,  $A_0 = 150$  K, as well as  $\nu = 0.7$ ,  $A_0 = 170$  K;  $\nu = 0.6$ ,  $A_0 = 145$  K are equally good in terms of describing the susceptibility. The fact that the classical exponent  $\frac{1}{2}$  coming from our simple high-temperature treatment allows for an acceptable fit of experimental susceptibility is pretty remarkable. We assume at this point for the sake of simplicity that the phase with the finite qDoS at the zero energy is the 1D-RVB one with the nonvanishing  $\zeta_c$ . Then using the zero temperature limiting value of this OP  $\zeta_c = \frac{1}{\pi}$  [3] we get  $J_c = 1310$  K. This nicely agrees with the original estimate of [1] (*ca.* 1000 K) and is more or less supported by other sources [8]. That is also what one can intuitively expect relying on the Goodenough-Kanamori rules [7].<sup>2</sup> Using it in the high-temperature estimate for the critical temperature eq. (6) we obtain for the highest critical temperature (that of the transition from the Curie paramagnetic to the 1D-RVB state) the value  $\theta_c^{\text{crit}} = 490$  K, which lies fairly above the decomposition temperature [1]. In case the Q1D-RVB phase is assumed to be responsible for the Pauli paramagnetism we take  $J_{ac} = 1400$  K as a plausible estimate. With use of it the highest critical temperature  $\theta_{c,ac}^{\text{crit}} = 435$  K is as well high enough. In that sense these estimates are consistent. For the exchange parameter  $J_a$  we notice that its values is pretty stable. Using eq. (6) for the temperature  $\theta_{c \rightarrow c,a}^{\text{crit}} = 95$  K of the pseudogap opening in the 1D-RVB phase, we arrive to a reasonable value of  $J_a = 550$  K. On the other hand considering this critical value as the critical temperature  $\theta_{c,ac \rightarrow c,a,ac}^{\text{crit}}$  given by eq. (8) yields  $J_a = 560$  K which shows pretty good consistency between two options of defining the Pauli paramagnetic phase.

## 3.2 Structure manifestations of transitions between RVB phases

### 3.2.1 Theory

Previously [5, 6] we were able to relate the RVB OPs and the lattice constants through "magnetostriction" - the linear coupling of the structure parameters with the exchange parameters. These moves absolutely apply in the present

---

<sup>2</sup>Our previous estimate [4] of 2300 K looks out to be somewhat exaggerated.

model with three exchange parameters and respective OPs. We assume as previously a linear relationship between the exchange parameters  $J_\tau$  and geometry parameters  $\rho_\lambda$ :

$$J_\tau = J_{\tau 0} + \sum_{\lambda} J'_{\tau, \lambda} \rho_\lambda. \quad (12)$$

Following [18] we assume that zeroes of  $\rho$ 's correspond to a hypothetical structure the CuNCN crystal would have provided the exchange interactions  $J_\tau$  are turned off. Deformation of this hypothetical structure requires the elastic energy

$$\frac{1}{2} \sum_{\mu\lambda} K_{\mu\lambda} \rho_\mu \rho_\lambda \quad (13)$$

for each nearest neighbor Cu-Cu pair. The observed geometry of the crystal where the exchange interactions result in formation of one of the RVB phases corresponds to the minimum with respect to  $\rho_\lambda$  of the free energy eq. (5) to which the elastic energy eq. (13) is added and the exchange parameters are replaced according to eq. (12) :

$$\frac{\partial F}{\partial \rho_\lambda} + \sum_{\mu\lambda} K_{\mu\lambda} \rho_\mu = 0. \quad (14)$$

Using the special form of the RVB free energy  $F$  (eq. (5)) we arrive to the explicit expression

$$\rho_\mu = \sum_{\lambda} (K)_{\mu\lambda}^{-1} \left( \sum_{\tau} A_{\tau} \zeta_{\tau}^2 J'_{\tau, \lambda} \right), \quad (15)$$

- the sought relation between the RVB OPs and their structure manifestations ( $A_\tau$  are numerical coefficients: 3 for  $\tau = a, c$ ; 6 for  $\tau = ac$ ) which further generalizes the famous bond-length-bond-order relation to the RVB states. Details are explained in Appendix D.

### 3.2.2 Synchrotron measurements on CuNCN as explained by RVB phase transitions

Now we can formulate what one could expect in the structural studies provided CuNCN undergoes transitions between various RVB phases. The vanishing OP's do not have any effect on the crystal structure. On the other

hand, a transition accompanied by splitting from zero of some OP will be manifested in the structure changes as prescribed by eq. (15). The sign of the effect is controlled by that of the magnetostriction parameters  $J'_{\tau,\lambda}$ . The temperature dependence of the structure described by the parameters  $\rho_\lambda$  is thus that of the relevant combination of the squares of the corresponding OPs, which can be different in different phases. Previously [5, 6] we could relate the experimental data on the anomalous temperature dependence of the lattice parameter  $a$  with the 1D-RVB to 2D-RVB phase transition of the anisotropic triangular Heisenberg model as accompanied by the opening of the gap in the quasiparticle spectrum in the  $a$ -direction. However, the experiment [6] showed some anomalies for the lattice parameter  $c$  at the temperature of the tentative 1D-RVB to 2D-RVB phase transition ( $80 \div 100$  K) and some more irregularities either in the  $a$ - or in the  $c$ -directions at  $ca.$  30 K. We also already mentioned above that the system of the exchange parameters of the anisotropic triangular Heisenberg model was not particularly intuitive.

The results of the structural studies related to the lattice parameter  $a$  are shown in Fig. 5. We do not directly apply the general formula eq. (15), but, first, take into account the approximately diagonal form of the inverse matrix of the force constants as derived in Appendix E and thus conclude that the structure manifestations in the  $a$ - and  $c$ -directions are independent. Since the exchange parameters are sums of contributions of many superexchange paths one can expect that they depend on all types of interatomic separations that is the magnetostriction constants  $J'_{\tau,\lambda}$  with  $\tau = a, c, ac$  and  $\lambda = a, c$  are not vanishing for all combinations of  $\tau$  and  $\lambda$ . It seems, however, to be reasonable, that the exchange constant  $J_a$  is not dependent on the deformation in the  $c$ -direction and thus  $J'_{a,c} = 0$ . Under these assumptions the structural manifestations in the  $a$ -direction decouple and can be recovered by using  $\tau, \lambda = a, \rho_a = \delta a = (a - a_0)$  in eq. (15). Like previously [5, 6] we conclude that the equilibrium value of  $\delta a$  in the RVB-phase with two pseudogaps must be proportional to the squared OP  $\zeta_a$ . Due to its direct relation with the pseudogap measured in the EPR experiments [4] we can relate two observed quantities: the deformations and the temperature dependent activation energy (the pseudogap  $A(\theta)$ ) in the quasi-Arrhenius regime:

$$\delta a = \frac{J'_{a,a}}{3K_{a,a}J_a^2} A(\theta)^2 \quad (16)$$

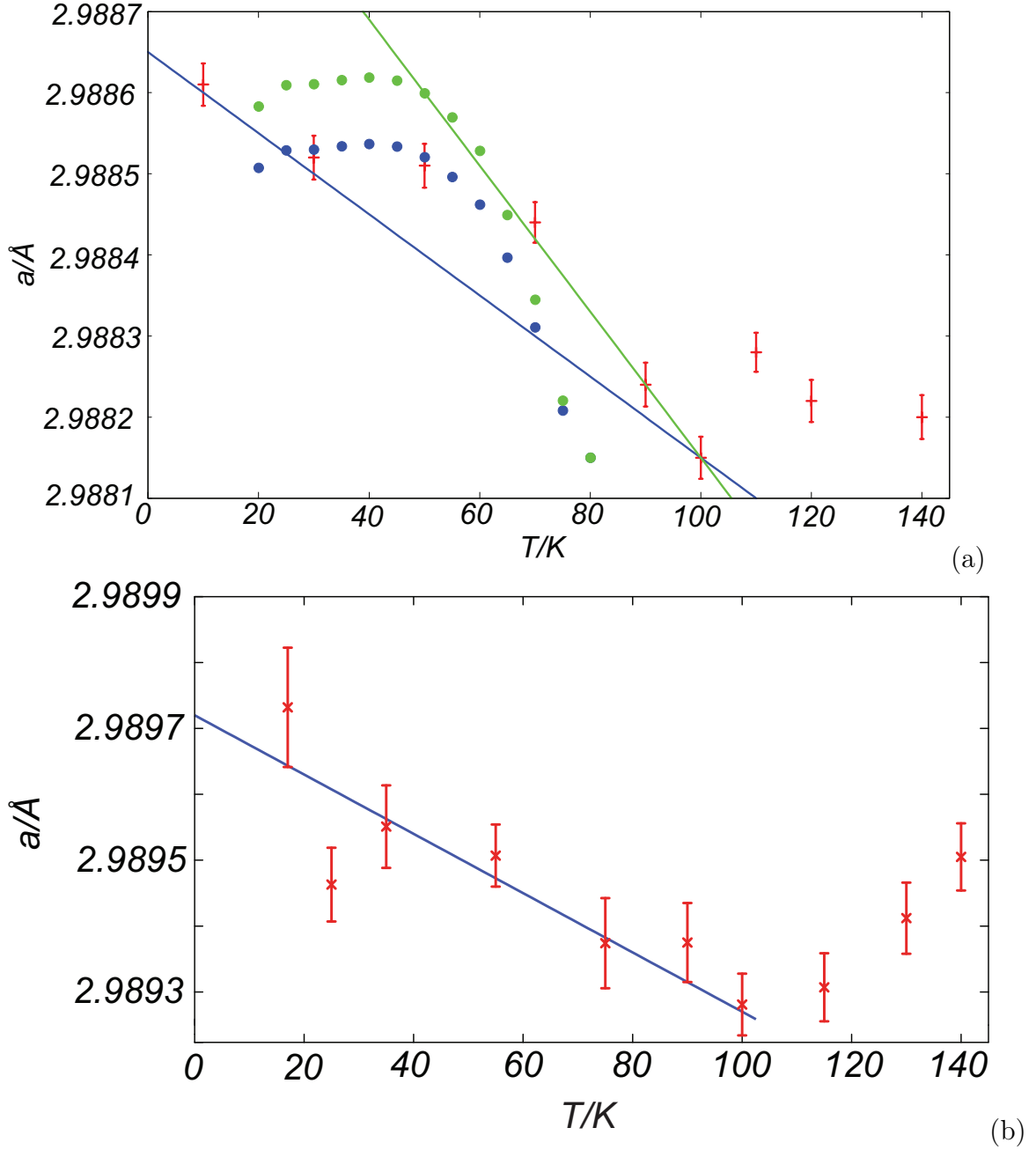


Figure 5: The temperature dependence of the  $a$ -lattice constant as extracted (a) from synchrotron experiment[6] (red dashes with error bars) as confronted with the  $\zeta_a^2$  values extracted from the ESR experiment and multiplied by a suitable constant  $J'_{a,a}/K_{aa} = 0.08 \text{\AA}$  (blue dots) or confronted with the linear model eq. (16) with the parameters  $\theta^{\text{crit}} = 100 \text{ K}$ ,  $\nu = 0.5$ ,  $A_0 = 140 \text{ K}$  extracted from one of the magnetic susceptibility fits; (b) from the neutron experiment[17] (red crosses with error bars) and confronted with the linear model eq. (16).

The crucial point is the sign of the effect. At the first glance the situation seems to be counterintuitive since in order to conform with the experiment (increase of the  $a$ -parameter in the 2D-RVB phase with two two-pseudogaps as compared to the (Q)1D-RVB phase (2, red - or 5, magenta) the exchange parameter  $J_a$  has to increase with the increase of the Cu-Cu interatomic separation. However, the effective value of the (antiferromagnetic) exchange parameter  $J_a$  is a sum of numerous contributions of different signs:

$$J_a = J_a(\text{antiferro}) - J_a(\text{ferro}) > 0,$$

where both  $J_a(\text{antiferro})$  and  $J_a(\text{ferro})$  are positive. The antiferromagnetic contribution is accumulated by summing up contributions from numerous superexchange paths and is weakly affected by the Cu-Cu interatomic separation since no direct matrix elements between the states of the two Cu atoms affects  $J_a(\text{antiferro})$ . By contrast the ferromagnetic contribution strongly depends on the angle  $\widehat{\text{CuNCu}}$  (see Refs. [7, 21]) and in the range of  $\widehat{\text{CuNCu}} > 90^\circ$ , which is the case for CuNCN, decreases while the  $\widehat{\text{CuNCu}}$  angle and thus the Cu-Cu separation increases. Respectively the effective antiferromagnetic exchange parameter  $J_a$  increases while the counterpoising ferromagnetic contribution decreases. This explains the overall positive sign of  $J'_{a,a}$  and thus the experimental fact of increase of the lattice parameter  $a$  in the phase with the pseudogap developing in the  $a$ -direction.

The quantitative agreement (shown in Fig. 5(a) by blue and green dots) is achieved by confronting the amplitude of the structure effect  $4 \cdot 10^{-4} \text{ \AA}$  [6] in the  $a$ -direction with the zero temperature limit of the pseudogap  $A(\theta \rightarrow 0)$  of *ca.* 70 K [4]. The problem with the latter estimate is that it is determined within somewhat different model [4, 5]. Alternatively we take the value of  $A_0 = 140 \text{ K}$  and the corresponding classical value of the exponent  $\nu = \frac{1}{2}$  as a plausible estimate for the zero temperature limit for the pseudogap and with the above value  $J_a = 560 \text{ K}$  we get  $\zeta_a(\theta \rightarrow 0) = 0.08$ . Then the ratio of effective constants finally responsible for the spin-phonon coupling is  $J'_{a,a}/K_{aa} = 0.19 \text{ \AA}$ . Combining this with the value of the force constant  $K_{aa}$  derived in Appendix E we can now evaluate  $J'_{a,a}$  to be *ca.* 12000 K/ $\text{\AA}$  which seems to fairly fit the expectations.

The synchrotron experiment was subject to a heavy and unfair criticism. Thus the neutron diffraction study of the temperature dependence of the CuNCN structure have been performed [17]. The results concerning the  $a$  lattice parameter are shown in Fig. 5(b). The most remarkable is that the

amplitude of the structure change as measured in the neutron scattering coincides with that coming from the synchrotron one:  $4 \cdot 10^{-4}$  Å. That means that our previous estimates of the parameters rationalizing the synchrotron and ESR data remain valid. In Fig. 5(a), (b) the experimental data fairly lie on a straight line in the temperature range between 100 K (the measured minimum of  $a$  determined by the neutron diffraction and somewhat less characteristic for the synchrotron data) and 30 K. This agrees with an assumption that in a rather wide range the temperature dependence of the OPs follow the standard temperature behavior with the classical value of the critical exponent  $\nu = \frac{1}{2}$  since according to our treatment eqs. (15), (16) the lattice parameters must obey the temperature evolution with the exponent  $2\nu$  *i.e.* be linear, as observed. This, however, changes to somewhat more chaotic behavior at *ca.* 30 K. This incidentally corroborates with the temperature run of the  $c$  lattice parameter measured in the synchrotron experiment [6] (Fig. 6) which did not receive due attention so far. As one can see the lattice parameter  $c$  generally (almost linearly) decreases with temperature. It shows some irregularities (not changing the sense of the run) about  $80 \div 100$  K, where the magnetic susceptibility changes from the quasi-Pauli to the quasi-Arrhenius regime due to opening the pseudogap in the  $a$ -direction. However, the sense of the temperature run of  $c$  changes at 30 K where the lattice parameter  $a$  starts to show irregularities as well.

In order to rationalize the low-temperature behavior of the lattice parameter  $c$  and eventually of  $a$  we introduce one more geometry variable  $2\rho_c = \delta c = c - c_0$  and apply the general relation eq. (15) and by this show that the variation of two lattice parameters is:

$$\begin{pmatrix} \delta a \\ \delta c \end{pmatrix} = \frac{3}{|K|} \begin{pmatrix} (K_{c,c}J'_{a,a} - 2K_{ac}J'_{a,c}) \zeta_a^2 + (K_{c,c}J'_{c,a} - 2K_{ac}J'_{c,c}) \zeta_c^2 \\ (-K_{ac}J'_{a,a} + 2K_{a,a}J'_{a,c}) \zeta_a^2 + (-K_{ac}J'_{c,a} + 2K_{a,a}J'_{c,c}) \zeta_c^2 \end{pmatrix}, \quad (17)$$

where we denote by  $|K|$  the determinant of the 2x2 matrix of the force constants and make use of our previous consideration allowing to neglect the OP  $\zeta_{ac}$ .

In order to qualitatively understand the temperature run of the lattice parameters  $a$  and  $c$  formally given by eq. (17) we take a closer look at the lower-temperature range of the parameter phase diagram Fig. 3. There one sees that below the octal point the thermal evolution consists *en gros* in squeezing out all the phases by the 2D-RVB phase with vanishing  $\zeta_{ac}$  (7 - orange). The 2D-RVB phase with three nonvanishing OP's (8 - yellow) is

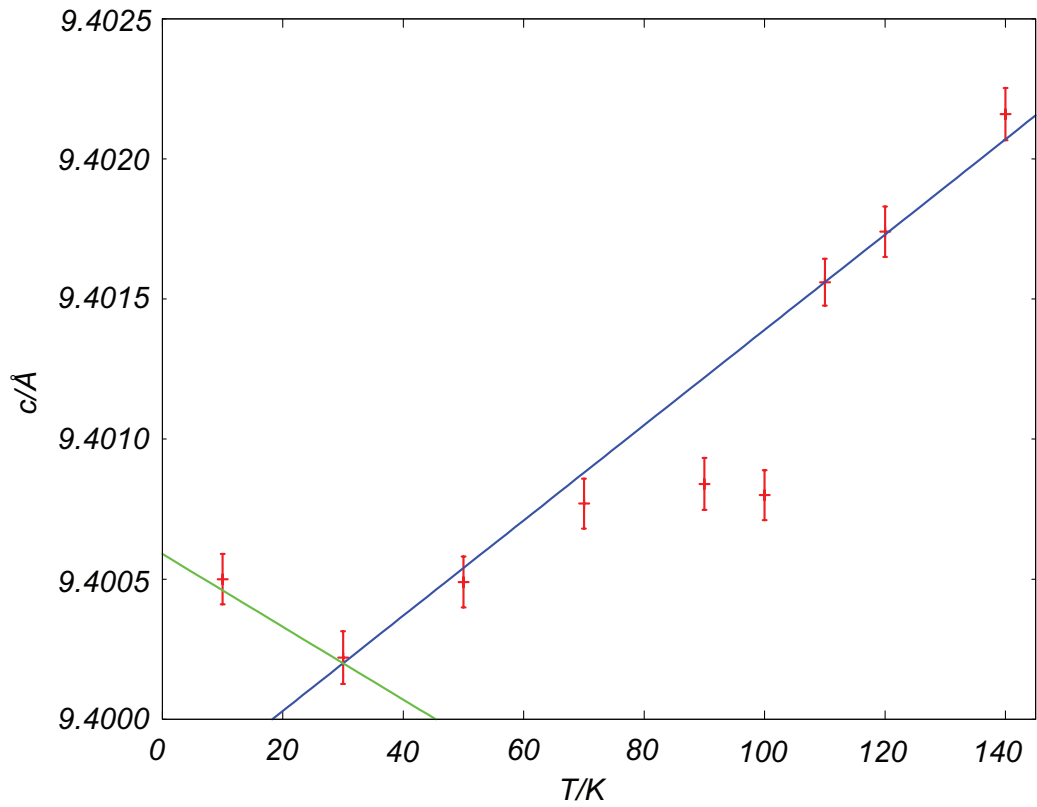


Figure 6: The temperature dependence of the  $c$ -lattice constant as extracted from the synchrotron experiment [6].

Table 2: Temperature dependencies of the OPs for possible phases of CuNCN in the high-temperature approximation of the  $c$ - $a$ - $ca$ -RVB model. The areas of the existence of the corresponding phases are given by the condition of positiveness of the expressions under the square roots.

Color code	OP's <i>vs.</i> $\theta$
Magenta	$\begin{cases} \zeta_a = 0 \\ \zeta_c = \frac{4\theta}{3J_c} \sqrt{1 - \theta/\theta_{c,ac}^{\text{crit}}} \\ \zeta_{ac} = \frac{8}{3} \sqrt{\frac{2}{3} \frac{\theta}{J_{ac}} \sqrt{\frac{\theta(J_{ac}-J_c)}{J_{ac}J_c}}} \end{cases} \quad \theta_{c,ac}^{\text{crit}} = \frac{3J_{ac}J_c}{8(3J_{ac}-2J_c)}$
Yellow	$\begin{cases} \zeta_a = \frac{4\theta}{3J_a} \sqrt{1 - \theta/\theta_{c,ac \rightarrow a,c,ac}^{\text{crit}}} \\ \zeta_c = \frac{4\theta}{3J_c} \sqrt{1 - \theta/\theta_{a,ac \rightarrow a,c,ac}^{\text{crit}}} \\ \zeta_{ac} = \frac{4}{3} \sqrt{\frac{1}{3} \frac{\theta}{J_{ac}} \sqrt{\theta/\theta_{a,c,ac}^{\text{crit}} - 1}} \end{cases} \quad \begin{aligned} \theta_{c,ac \rightarrow a,c,ac}^{\text{crit}} &= \frac{3J_{ac}J_a}{8(3J_{ac}-2J_a)} \\ \theta_{a,ac \rightarrow a,c,ac}^{\text{crit}} &= \frac{3J_{ac}J_c}{8(3J_{ac}-2J_c)} \\ \theta_{a,c,ac}^{\text{crit}} &= \text{eq. (9)} \end{aligned}$
Orange	$\begin{cases} \zeta_a = \frac{4\theta}{\sqrt{15}J_a} \sqrt{1 - \theta/\theta_{c \rightarrow a,c}^{\text{crit}}} \\ \zeta_c = \frac{4\theta}{\sqrt{15}J_c} \sqrt{1 - \theta/\theta_{a \rightarrow a,c}^{\text{crit}}} \\ \zeta_{ac} = 0 \end{cases} \quad \begin{aligned} \theta_{c \rightarrow a,c}^{\text{crit}} &= \frac{3J_aJ_c}{8(3J_c-2J_a)} \\ \theta_{a \rightarrow a,c}^{\text{crit}} &= \frac{3J_aJ_c}{8(3J_a-2J_c)} \end{aligned}$

transient, its parameters' area is never large and it is subject to deformations and displacements under the “pressure” of the phase 7. The same “pressure” squeezes the area of existence of the Q1D-RVB phase 5 (magenta) as well. Assuming the position of CuNCN on the parameters phase diagram Fig. 3 within the magenta phase, but close and somewhat below the quadruple point of the phases 2, 5, 7, and 8 (red, magenta, orange, and yellow) in the rightmost graph in the middle row one can see on the following slices the following sequence of transitions between the RVB phases:

$$\begin{array}{ccccc} \text{Q1D - RVB} & \rightarrow & \text{2D - RVB} & \rightarrow & \text{2D - RVB} \\ \zeta_c, \zeta_{ac} & \rightarrow & \zeta_c, \zeta_{ac}, \zeta_a & \rightarrow & \zeta_c, \zeta_a \\ \text{magenta} & \rightarrow & \text{yellow} & \rightarrow & \text{orange} \end{array} .$$

The thermal dependence of the OPs *within* these phases is described by the formulae of Table 2. One should not expect that these expressions derived from the high-temperature expansion for the free energy are exactly valid at low-temperature. Specifically, the prefactors  $\theta$  should not be taken seriously since we expect that the  $\zeta_{a,c}$  OPs flow to some finite values as temperature



flows to zero, although splitting from zero values at the critical temperatures given next to them. Upto that uncertain factor the temperature dependence of the OPs in three presumably observed phases is as follows. As we explained earlier, since the exchange parameters satisfy the condition  $J_{ac} \gtrsim J_c$  the OP  $\zeta_{ac}$  is always small and decreases with decreasing temperature, thus we do not consider it explicitly further. The OP  $\zeta_c$  should in principle increase either in the magneta or in yellow phases, but we assume that in the interesting temperature range  $\theta \ll \theta_{c,ac}^{\text{crit}} = \theta_{a,ac \rightarrow a,c,ac}^{\text{crit}} = 435$  K it has almost reached its zero temperature limit and does not significantly change any more.<sup>3</sup> The OP  $\zeta_a$  splits from zero at the critical temperature of  $\theta_{c,ac \rightarrow a,c,ac}^{\text{crit}} \approx 100$  K (transition to the yellow phase) which affects the  $a$  lattice parameter as explained above. In the general setting eq. (17), but under previous assumption of  $J'_{a,c} = 0$  the temperature independent  $\zeta_c^2$  does not contribute to the visible variation of the lattice constants. However, the lattice parameter  $c$  turns out to be sensitive to the pseudogap opening in the  $a$  direction through the off-diagonal element of the the inverse matrix of the force constants. Particularly remarkable is the fact that the effect on the  $c$  is predicted to have the sign opposite to that on  $a$  ( $a$  increases,  $c$  decreases), as observed. Finally at the lowest accessible critical temperature  $\theta_{a,c,ac}^{\text{crit}}$  eq. (9) a transition to the orange phase takes place. A word of caution needs to be said here: the present set of the exchange parameters yields very narrow temperature range where the transient (yellow) phase can exist. We assume that eq. (9) strongly overestimates this temperature (92 K), which must be considerably lower (*ca.* 30 K) since one cannot rely upon the results of the high-temperature expansion any more. For obtaining more reliable estimates one needs to know at least the zero temperature limit of the  $a$ - $c$ - $ca$  model which is yet to be done. However, we assume that the general shape of the phase diagram is correctly reproduced by the high-temperature expansion and proceed within this setting. The evanescence of  $\zeta_{ac}$  at  $\theta_{a,c,ac}^{\text{crit}}$  whatever it is affects neither the bandwidth, since this OP is never large, nor the character of the temperature dependence of  $\zeta_a$ , although the variation of the slope can be as well expected. However, at this phase transition a remarkable change can be expected to the character of the temperature dependence of  $\zeta_c$ . Namely, it switches from increase to decrease. This happens because of an instantaneous change of

---

<sup>3</sup>Possible minor effect of increase of  $\zeta_c$  produces no visible temperature dependence of the Q1D-RVB quasiparticle bandwidth due to decrease of  $\zeta_{ac}$  since these two contributions changing in opposite directions compensate variations of each other.

its reference temperature shown in Table 2 from positive  $\theta_{a,ac \rightarrow a,c,ac}^{\text{crit}}$  to  $\theta_{a \rightarrow a,c}^{\text{crit}}$  which is *negative* (and much smaller by absolute value: *ca.*  $-300$  K) in the relevant area of the exchange parameters' ( $J_{ac} \gtrsim J_c > J_a$ ) space. Together changing the the sign and the magnitude of the reference temperature causes the change of the temperature run of the OP  $\zeta_c$  which starts to decrease in the orange phase and through eq. (17) affect the temperature behavior of the lattice parameters  $a$  and  $c$ . This tentatively and qualitatively explains the anomalies observed in Figs. 5 and 6 although the available amount of experimental data does not suffice to reliably estimate quite a few magnetostriction and other parameters required for at least semiquantitative description. In the minimal setting: *i.e.* neglecting the off-diagonal elements of the inverse matrix of force constants and the off-diagonal magnetostriction terms we immediately obtain

$$\delta c = \frac{6J'_{c,c}}{K_{c,c}} \zeta_c^2$$

which allows to at least conclude that the magnetostriction parameter  $J'_{c,c}$  has intuitively understandable sign: it is negative since  $\delta c$  turns to be positive when the variation of OP  $\zeta_c$  is negative.

## 4 Conclusion

A new form of the frustrated spatially anisotropic antiferromagnetic Heisenberg Hamiltonian close to the popular  $J_1 J_2 J_3$  model with exchange parameters  $J_c$ ,  $J_a$ , and  $J_{ac}$  extended along the  $c$ ,  $a$ , and  $a \pm c$  directions of a two-dimensional rectangular lattice is proposed. When applied to model fascinating physics of copper carbodiimide (CuNCN) it explains the absence of magnetic order in CuNCN down to 4 K by assuming resonating valence bond (RVB) character of the emerging phases. The quasiparticle spectrum of the RVB model of the proposed Hamiltonian shows three principal regimes: (i) a state with two pairs of lines of nodes, (ii) states with a pair of lines of nodes (termed as 1D- and Q1D-RVB states), (iii) states with two pseudogaps and four nodal points (2D-RVB states). Extraordinary rich parameters-temperature phase diagram of the model contains eight different phases whose magnetic behavior includes Curie and quasi-Pauli paramagnetism (1D- and Q1D-RVB phases), and (pseudo)gapped (quasi-Arrhenius) paramagnetism (2D-RVB phases). Adding magnetostriction and elastic terms to the free energy of the model explains the the temperature

dependence of the CuNCN crystal structure by assuming that a sequence of transitions between different RVB phases occurs in CuNCN while temperature decreases. Confronting the model with the magnetic susceptibility and structure (both synchrotron and neutron) data recorded as functions of temperature in the range between *ca.* 10 and 200 K shows a remarkably good agreement between the theoretical predictions and the experiment which is reached by ascribing the values of the model parameters which are intuitively acceptable both in terms of their absolute magnitudes, relative values, and the character of their geometry dependence.

## Acknowledgments

This work has been performed with the support of Deutsche Forschungsgemeinschaft. In addition, we acknowledge the Russian Foundation for Basic Research for the financial support dispatched to ALT through the grant No. 13-03-90430. Dr. Andrej Zorko of Jožef Stefan Institute (Ljubljana, Slovenia) is acknowledged for sending numerical data on the  $T$ -dependence of the energy gap as extracted from the ESR measurements [4] as well as of the data on the ESR susceptibility. Prof. Dr. U. Ruschewitz of the University of Cologne is acknowledged for sending numerical data on the  $T$ -dependence of the lattice parameters as derived from the synchrotron experiments [6].

## References

- [1] X.-H. Liu, R. Dronskowski, R.K. Kremer, M. Ahrens, C.-D. Lee, M.-H. Whangbo, **J. Phys. Chem. C** 112 (2008) 11013.
- [2] H. Xiang et al., **J. Phys. Chem. C** 113 (2009) 18891.
- [3] A.L. Tchougréeff, R. Dronskowski. **arXiv**:1008.0182.
- [4] A. Zorko, P. Jeglič, A. Potočnik, D. Arčon, A. Balčytis, X. Liu, A.L. Tchougréeff, R. Dronskowski. **Phys. Rev. Lett.** 107 (2011) 047208.
- [5] A.L. Tchougréeff, R. Dronskowski. **arXiv**:1111.7210.

- [6] A.L. Tchougréeff, X. Liu, P. Müller, W. van Beek, U. Ruschewitz, R. Dronskowski. **J. Phys. Chem. Lett.** 3 (2012) 3360-3366.
- [7] J.B. Goodenough. Magnetism and the Chemical Bond. Interscience-Wiley, New York, 1963.
- [8] A.A. Tsirlin, A. Maisuradze, J. Sichelschmidt, W. Schnelle, P. Höhn, R. Zinke, J. Richter, H. Rosner. **arXiv:1203.4706v1**.
- [9] M. Ogata. **J. Phys. Soc. Jap.** 72 (2003) 1839.
- [10] M. Ogata and H. Fukuyama. **Rep. Progr. Phys.** 71 (2008) 036501.
- [11] P. Hauke, T. Roscilde, V. Murg, J. I. Cirac, R. Schmied. **New J. Phys.**, 13 (2011) 075017; M. Kohno, L. Balents, O.A. Starykh. **J. Phys.: Conf. Ser.**, 145 (2009) 012062; P. Chandra, B. Doucot, **Phys. Rev. B**, 38 (1988) 9335; M. Mambrini, A. Läuchli, D. Poilblanc, F. Mila. **Phys. Rev. B**, 74 (2006) 144422; F. Figueirido, A. Karlhede, S. Kivelson, S. Sondhi, M. Roček, D.S. Rokhsar. **Phys. Rev. B**, 41 (1989) 4619; N. Read, S. Sachdev. **Phys. Rev. Lett.**, 66 (1991) 1773; J. Ferrer. **Phys. Rev. B**, 47 (1993) 8769.
- [12] Y. Hayashi and M. Ogata. **J. Phys. Conf. Ser.** 150 (2009) 042053.
- [13] Y. Hayashi and M. Ogata. **arXiv:0704.1313v1**; Y. Hayashi and M. Ogata, **J. Phys. Soc. Jpn.** 76 (2007) 053705.
- [14] A.L. Tchougréeff, R. Hoffmann. **J. Phys. Chem.** 96 (1992) 8993-8998.
- [15] L.K. Grigor'eva, N.S. Lidorenko, E.L. Nagaev, S.P. Čížik. **J. Exp. Theor. Phys.**, 91 (1986) 1050 [in Russian].
- [16] V.N. Tutubalin. Probability theory and stochastic processes. MSU Publ., Moscow, 1992 [in Russian].

- [17] H. Sawinski, A. Houben, P. Jacobs, P. Müller, A. Tchougréeff, R. Dronskowski. Reinvestigating the crystal structure of CuNCN. Poster. German Neutron Scattering Conference, Bonn, Germany 24 - 26.09.2012.
- [18] I. A. Misurkin, A. A. Ovchinnikov. **J. Struct. Chem.**, 5 (1965) 888 [in Russian]; I. A. Misurkin, A. A. Ovchinnikov. **Opt. Spectr.**, 16, 228 (1964) [in Russian]; I. A. Misurkin, A. A. Ovchinnikov, **Usp. Khim.**, 46, 1833 (1977) [in Russian].
- [19] L.D. Landau, E.M. Lifshits. Theoretical Physics VII. Elasticity Theory. [in Russian].
- [20] R. Stoffel. Private communication.
- [21] M.A. Atanasov, S. Angelov, I. Mayer. **Solid State Commun.** 56 (1985) 743; M.A. Atanasov, S. Angelov, I. Mayer. **J. Mol. Struct. (THEOCHEM)** 1989, 187, 23.

## A Equations of motion and self consistency equations.

Equations of motion are based on the Heisenberg representation in which each operator obeys the following:

$$i\hbar\dot{A} = [A, H] \quad (18)$$

where  $[..., ...]$  stands for the commutator and  $\dot{\phantom{A}}$  for the time derivative. Applying this to the creation and annihilation operators  $c_{\mathbf{r}\sigma}^+$  ( $c_{\mathbf{r}\sigma}$ ) and performing commutation, mean field decoupling and Fourier transformation as done previously [3] results in mean field equations of motion for them:

$$\begin{aligned} i\hbar\dot{c}_{\mathbf{k}\sigma} &= -\frac{3}{2} \sum_{\tau} J_{\tau} \xi_{\tau} \cos(\mathbf{k}\tau) c_{\mathbf{k}\sigma} - \frac{3}{2} \sum_{\tau} J_{\tau} \Delta_{\tau} \cos(\mathbf{k}\tau) c_{-\mathbf{k}-\sigma}^+ \\ i\hbar\dot{c}_{\mathbf{k}\sigma}^+ &= \frac{3}{2} \sum_{\tau} J_{\tau} \xi_{\tau} \cos(\mathbf{k}\tau) c_{\mathbf{k}\sigma}^+ - \frac{3}{2} \sum_{\tau} J_{\tau} \Delta_{\tau}^* \cos(\mathbf{k}\tau) c_{-\mathbf{k}-\sigma} \end{aligned} \quad (19)$$

These latter reduces to the set of  $2 \times 2$  eigenvalue problems for each wave vector  $\mathbf{k}$ :

$$\begin{pmatrix} \xi_{\mathbf{k}} & \Delta_{\mathbf{k}} \\ \Delta_{\mathbf{k}}^* & -\xi_{\mathbf{k}} \end{pmatrix} \begin{pmatrix} u_{\mathbf{k}} \\ v_{\mathbf{k}} \end{pmatrix} = E_{\mathbf{k}} \begin{pmatrix} u_{\mathbf{k}} \\ v_{\mathbf{k}} \end{pmatrix}$$

with

$$\begin{aligned} \xi_{\mathbf{k}} &= -3 \sum_{\tau} J_{\tau} \xi_{\tau} \cos(\mathbf{k}\tau) \\ \Delta_{\mathbf{k}} &= 3 \sum_{\tau} J_{\tau} \Delta_{\tau} \cos(\mathbf{k}\tau) \end{aligned}$$

(summation over  $\tau$  extends to  $\tau_i; i = 1 \div 4$ ) which results in the eigenvalues:

$$E_{\mathbf{k}} = \pm \sqrt{\xi_{\mathbf{k}}^2 + |\Delta_{\mathbf{k}}|^2}$$

whose eigenvectors are combinations of the annihilation and creation operators with the coefficients  $u_{\mathbf{k}}, v_{\mathbf{k}}$ . This set of equations closes by the selfcon-

sistency conditions:

$$\begin{aligned}\xi_\tau &= -\frac{1}{2N} \sum_{\mathbf{k}} \exp(i\mathbf{k}\tau) \frac{\xi_{\mathbf{k}}}{E_{\mathbf{k}}} \tanh\left(\frac{E_{\mathbf{k}}}{2\theta}\right) \\ \Delta_\tau &= \frac{1}{2N} \sum_{\mathbf{k}} \exp(-i\mathbf{k}\tau) \frac{\Delta_{\mathbf{k}}}{E_{\mathbf{k}}} \tanh\left(\frac{E_{\mathbf{k}}}{2\theta}\right)\end{aligned}\quad (20)$$

for the order parameters (OPs). The lattice symmetry considerations allow us to restrict ourselves by the OPs:  $\xi_a, \xi_c, \xi_{ac}; \Delta_a, \Delta_c, \Delta_{ac}$ . For the complex OPs we introduce a polar representation:

$$\Delta_\tau = \eta_\tau e^{i\varphi_\tau}.$$

The standard moves foreseen for the  $SU(2)$  symmetric solutions are used to exclude the cross terms in OPs from  $E_{\mathbf{k}}^2$  which leads to the system of equations:

$$\xi_\tau \xi_{\tau'} = -\eta_\tau \eta_{\tau'} \cos(\varphi_\tau - \varphi_{\tau'})$$

(three equations). Introducing the relative phases as:  $\theta_a = \varphi_a - \varphi_{ac}$ ;  $\theta_c = \varphi_c - \varphi_{ac}$  we arrive to the equations of the form:<sup>4</sup>

$$\begin{aligned}\xi_a \xi_c + \eta_a \eta_c \cos(\theta_a - \theta_c) &= 0 \\ \xi_a \xi_{ac} + \eta_a \eta_{ac} \cos \theta_a &= 0 \\ \xi_c \xi_{ac} + \eta_c \eta_{ac} \cos \theta_c &= 0\end{aligned}$$

similar to those derived in [9] which can be satisfied *e.g.* by setting

$$\begin{aligned}\xi_a \xi_c &= -\eta_a \eta_c \neq 0 \\ \theta_a &= \theta_c = \frac{\pi}{2} \\ \eta_{ac} &\neq 0; \xi_{ac} = 0\end{aligned}\quad (21)$$

Of course, the OPs can be also vanishing.

Under the above conditions the spectrum of quasiparticles acquires the form:

$$E_{\mathbf{k}}^2 = 9 (J_a^2 (\xi_a^2 + \eta_a^2) \cos^2 x + J_c^2 (\xi_c^2 + \eta_c^2) \cos^2 z + 4J_{ac}^2 (\xi_{ac}^2 + \eta_{ac}^2) \cos^2 x \cos^2 z)$$

where we set  $x = \mathbf{k}_x; z = \mathbf{k}_z$ .

---

<sup>4</sup>The consequences of setting  $\theta_c = \varphi_{ac} - \varphi_c$  and thus having the first equation in the form  $\xi_a \xi_c + \eta_a \eta_c \cos(\theta_a + \theta_c) = 0$ , which exactly coincides with [9], yet have to be studied. Most probably it brings up more degenerate phases with various phase angles.

## B High-temperature expansion.

At high temperature we can use an expansion:

$$\ln \left( 2 \cosh \left( \frac{E_{\mathbf{k}}}{2\theta} \right) \right) \approx \ln 2 + \frac{1}{2} \left( \frac{E_{\mathbf{k}}}{2\theta} \right)^2 - \frac{1}{12} \left( \frac{E_{\mathbf{k}}}{2\theta} \right)^4$$

which when inserted in eq. (5) integrates explicitly. For determining the critical temperatures to the first approximation it suffices to restrict ourselves by the second power terms. This results in an expression quadratic in  $\zeta_\tau$ . Combining thus obtained "kinetic" energy:

$$-2\theta \cdot \frac{9}{8\theta^2} \left( \frac{1}{2} J_a^2 \zeta_a^2 + \frac{1}{2} J_c^2 \zeta_c^2 + J_{ac}^2 \zeta_{ac}^2 \right),$$

with the potential energy terms from eq. (5) we get:

$$F_{\text{HT}} = \sum_{\tau} \left[ -\frac{9}{8\theta} J_{\tau}^2 + 3J_{\tau} \right] \zeta_{\tau}^2.$$

This result can be improved with use of the Ginzburg-Landau approximate free energy  $F_{\text{GL}}(\zeta_{\tau}, \theta)$  which involves the terms up to the fourth power in  $\zeta_{\tau}$ 's. They appear from the integration of the 4-th power of the spectrum which performs explicitly and yields the "kinetic" energy of the form:

$$\begin{aligned} & \frac{1}{768\theta^3} [36\zeta_a^2 J_a^2 (27\zeta_{ac}^2 J_{ac}^2 + 9\zeta_c^2 J_c^2 - 24\theta^2) \\ & + 243\zeta_a^4 J_a^4 + 3(36\zeta_{ac}^2 J_{ac}^2 (9\zeta_c^2 J_c^2 - 16\theta^2)) \\ & + 486\zeta_{ac}^4 J_{ac}^4 - 288\theta^2 \zeta_c^2 J_c^2 + 81\zeta_c^4 J_c^4] \end{aligned}$$

which together with the potential energy yields the free energy  $F_{\text{GL}}(\zeta_{\tau}, \theta)$  used for further analysis.

## C Quasiparticle densities of states in various RVB phases

In Section 2.2 we gave an impression of the complexity of the phase diagram of the RVB model with three exchange parameters. We also gave a brief description of the most characteristic features of the qDoS in various RVB



phases. Here we provide a brief sketch of the derivation of qDoS given in Table 1.

The definition of the qDoS reads:

$$g(\varepsilon) = \frac{1}{4\pi^2} \int_{BZ} \delta(\varepsilon - E_{\mathbf{k}}) d^2\mathbf{k}$$

Following Ref. [15] we insert the integral representation for the Dirac  $\delta$ -function:

$$\begin{aligned} g(\varepsilon) &= \frac{1}{2\pi} \frac{1}{4\pi^2} \int_{BZ} \int_{-\infty}^{\infty} dt \exp(it(\varepsilon - E_{\mathbf{k}})) d^2\mathbf{k} = \\ &= \frac{1}{2\pi} \int_{-\infty}^{\infty} dt \left[ \exp(it\varepsilon) \frac{1}{4\pi^2} \int_{BZ} \exp(-itE_{\mathbf{k}}) d^2\mathbf{k} \right]. \end{aligned}$$

For all phases having lines of nodes (those with numbers 2 - 6) the integration over one of the components of the wave vector  $\mathbf{k}$  in the BZ is performed and yields an intermediate result in terms of the the Bessel and Struve functions of arguments dependent on the Fourier transformation variable  $t$  and the remaining component of the wave vector  $\mathbf{k}$ . The Fourier transforms with respect to  $t$  can be done for the intermediate answers of that form. It yields integrands of the elliptic integrals over the remaining component of the wave vector  $\mathbf{k}$ . This solves the problem of calculationg the qDoS for the dispersion laws with the lines of nodes in the BZ. The results are given in respective cells of Table 1.

In order to cope with remaining two phases whose spectra contain only nodal points (numbers 7 and 8) one more trick, namely performing previous moves for the squared spectrum and thus obtaining the distribution of the states as a function of their squared energy solves the problem. The distribution of squares of the quasiparticle energies is:

$$\varrho(\varepsilon^2) = \frac{1}{4\pi^2} \int_{BZ} \delta(\varepsilon^2 - E_{\mathbf{k}}^2) d^2\mathbf{k}.$$

Then the sought qDoS is given by [16]:

$$g(\varepsilon) = 2\varepsilon\varrho(\varepsilon^2).$$

To obtain  $\varrho(\varepsilon^2)$  we again use the integral representation of the Dirac  $\delta$ -function:

$$\begin{aligned}\varrho(\varepsilon^2) &= \frac{1}{2\pi} \frac{1}{4\pi^2} \int_{BZ} \int_{-\infty}^{\infty} dt \exp(it(\varepsilon^2 - E_{\mathbf{k}}^2)) d^2\mathbf{k} = \\ &= \frac{1}{2\pi} \int_{-\infty}^{\infty} dt \left[ \exp(it\varepsilon^2) \frac{1}{4\pi^2} \int_{BZ} \exp(-itE_{\mathbf{k}}^2) d^2\mathbf{k} \right].\end{aligned}$$

Remarkably enough sequential integrations of the squared spectrum over one of the components of the wave vector  $\mathbf{k}$  and Fourier transformation with respect to  $t$  yield the expressions of the same form as integration of the spectrum itself: the Bessel function and an integrand of the elliptic integral. Thus the final intergration over the remainig component of the wave vector  $\mathbf{k}$  yields some elliptic integrals given in respective cells of Table 1.

## D Theory of the structural manifestations of the RVB states.

We start from the mechanic equilibrium condition of the crystal in a RVB phase:

$$\frac{\partial F}{\partial \rho_\lambda} + \sum_{\mu\lambda} K_{\mu\lambda} \rho_\mu = 0. \quad (23)$$

and notice that the free energy  $F$  given by eq. (5) has a special form. The first term (“kinetic” energy) is integral of a function of the dispersion law  $E_{\mathbf{k}}$  whose argument has the form:

$$\sum_{\tau} A_{\tau}^2 J_{\tau}^2 \zeta_{\tau}^2 f_{\tau}^2(\mathbf{k}),$$

where  $A_{\tau}$  are numerical coefficients (3 for  $\tau = a, c$ ; 6 for  $\tau = ac$ );  $f_{\tau}(\mathbf{k})$  are trigonometrical expressions ( $\cos \mathbf{k}_{\tau}$  for  $\tau = a, c$ ;  $\cos \mathbf{k}_a \cos \mathbf{k}_c$  for  $\tau = ac$ ). The “potential” energy contribution to the free energy eq. (5) is:

$$\sum_{\tau} A_{\tau} J_{\tau} \zeta_{\tau}^2.$$

Due to the above special form of the “kinetic” and “potential” energies the self-consistency equations for  $\zeta_\tau$  have the form:

$$\int_{BZ} \tanh\left(\frac{E_{\mathbf{k}}}{2\theta}\right) E'_{\mathbf{k}} A_\tau^2 J_\tau^2 \zeta_\tau f_\tau^2(\mathbf{k}) d^2\mathbf{k} = A_\tau J_\tau \zeta_\tau$$

each, to be solved simultaneously for all  $\tau$ . Apparently whatever (sub)set of  $\zeta_\tau = 0$  satisfies the equations. For the nonvanishing OPs the self-consistency equations acquire the form:

$$\int_{BZ} \tanh\left(\frac{E_{\mathbf{k}}}{2\theta}\right) E'_{\mathbf{k}} f_\tau^2(\mathbf{k}) d^2\mathbf{k} = \frac{1}{A_\tau J_\tau}. \quad (24)$$

Now we can turn to the structure determination. The derivative of the kinetic energy with respect to the geometry parameters  $\rho_\lambda$  reads:

$$-2 \sum_{\tau} A_\tau^2 \left( J_\tau \zeta_\tau^2 J'_{\tau,\lambda} + J_\tau^2 \zeta_\tau \frac{\partial \zeta_\tau}{\partial \rho_\lambda} \right) \int_{BZ} \tanh\left(\frac{E_{\mathbf{k}}}{2\theta}\right) E'_{\mathbf{k}} f_\tau^2(\mathbf{k}) d^2\mathbf{k}.$$

The value of the above integral for the equilibrium values of the OPs is given by the self-consistency conditions eq. (24). Thus the derivative of the kinetic energy rewrites:

$$-2 \sum_{\tau} A_\tau \left( \zeta_\tau^2 J'_{\tau,\lambda} + J_\tau \zeta_\tau \frac{\partial \zeta_\tau}{\partial \rho_\lambda} \right).$$

Combining this with the derivative of the potential energy and that of the elastic energy we get:

$$-2 \sum_{\tau} A_\tau \left( \zeta_\tau^2 J'_{\tau,\lambda} + J_\tau \zeta_\tau \frac{\partial \zeta_\tau}{\partial \rho_\lambda} \right) + \sum_{\tau} A_\tau \left( \zeta_\tau^2 J'_{\tau,\lambda} + 2J_\tau \zeta_\tau \frac{\partial \zeta_\tau}{\partial \rho_\lambda} \right) + \sum_{\mu\lambda} K_{\mu\lambda} \rho_\mu = 0.$$

The terms including the derivative  $\frac{\partial \zeta_\tau}{\partial \rho_\lambda}$  stemming from the kinetic and potential energies cancel each other: a remarkable consequence of the Hellmann-Feynman and virial theorems, which immediately results in:

$$- \sum_{\tau} A_\tau (\zeta_\tau^2 J'_{\tau,\lambda}) + \sum_{\mu\lambda} K_{\mu\lambda} \rho_\mu = 0,$$

which after some trivial algebra results in:

$$\rho_\mu = \sum_\lambda (K)_{\mu\lambda}^{-1} \left( \sum_\tau A_\tau \zeta_\tau^2 J'_{\tau,\lambda} \right). \quad (25)$$

## E Estimate of the force matrix from the elastic constants

Now we notice that the deformation tensor (for methods used for this and further evaluates see Ref. [19]) corresponding to the structure variation as described by the geometry deformation parameter  $\rho_a = \delta a$  has only one non-vanishing component  $u_{aa} = \delta a/a_0$ . The elastic energy of the unit cell under such deformation is:

$$\frac{1}{2} C_{aa,aa} a_0 b_0 c_0 \left( \frac{\delta a}{a_0} \right)^2 = 4 \times \frac{1}{2} K_{aa} (\delta a)^2,$$

where  $C_{aa,aa}$  is the corresponding element of the elasticity moduli tensor, the multiplier of 4 in the right hand side takes into account that each unit cell of CuNCN contains four Cu-Cu interactions along the  $a$ -direction, and  $a_0$ ,  $b_0$ , and  $c_0$  are the orthorhombic (?) lattice constants, so that we get the estimate:

$$K_{aa} = \frac{b_0 c_0}{4 a_0} C_{aa,aa}.$$

Completely analogous consideration of the deformation parameter  $2\rho_c = \delta c$ , yields the deformation tensor with single nonvanishing component  $u_{cc} = \delta c/c_0$  (the factor 2 takes care of the fact that in the structure shown in Fig. 1 the Cu-Cu distance in the  $c$  direction fits twice in the unit cell) yields:

$$\frac{1}{2} C_{cc,cc} a_0 b_0 c_0 \left( \frac{\delta c}{c_0} \right)^2 = \frac{1}{2} C_{cc,cc} a_0 b_0 c_0 \left( \frac{2\rho_c}{c_0} \right)^2 = 4 \times \frac{1}{2} C_{cc,cc} \frac{a_0 b_0}{c_0} \rho_c^2 = 4 \times \frac{1}{2} K_{cc} \rho_c^2,$$

where the factor 4 in the rightmost expression as in the case of the lattice direction  $a$  takes into account the presence of the four Cu-Cu bonds in the  $ab$  cross section. Thus:

$$K_{cc} = \frac{a_0 b_0}{c_0} C_{cc,cc}.$$

In the general case when both lattice parameters  $a$  and  $c$  change although not  $b$  and neither of angles the deformation tensor has two nonvanishing

components  $u_{aa}$  and  $u_{cc}$  defined above. The energy of one unit cell under such deformation reads

$$a_0 b_0 c_0 \left( \frac{1}{2} C_{aa,aa} \left( \frac{\delta a}{a_0} \right)^2 + \frac{1}{2} C_{cc,cc} \left( \frac{\delta c}{c_0} \right)^2 + C_{aa,cc} \left( \frac{\delta a}{a_0} \right) \left( \frac{\delta c}{c_0} \right) \right)$$

Singling out the remaining off-diagonal term we write:

$$b_0 C_{aa,cc} \delta a \delta c = b_0 C_{aa,cc} 2 \rho_a \rho_c = 4 \times 4 \times K_{ac} \rho_a \rho_c$$

where two factors of 4 in the rightmost term take into account the fact the four Cu-Cu bonds are extended from the given unit cell in either direction  $a$  or  $c$ . Thus

$$K_{ac} = \frac{b_0}{8} C_{aa,cc}$$

From the VASP calculations on CuNCN in various antiferromagnetic states we have for  $C_{aa,aa}$  the estimates of 195.6 or 181.3 GPa,  $C_{cc,cc}$  is 159.6 GPa, and  $C_{aa,cc}$  49.5 GPa [20]. Taking into account the SI units relations (1 GPa =  $10^9$  J/m<sup>3</sup>, 1 Å =  $10^{-10}$  m,  $k_B = 1.38 \cdot 10^{-23}$  J/K and the values of the lattice constants of CuNCN ( $a_0 = 2.99$ ,  $b_0 = 6.19$ ,  $c_0 = 9.41$  Å, see Refs. [1, 6]) we obtain the elastic constant  $K_{aa}$  to be in the range of 64100 to 69000 K/Å<sup>2</sup> (*i.e. ca.* 6 to 7 eV/Å<sup>2</sup>) pretty smaller than the characteristic values derived for analogous constant in polyenes [18], which one, however, could expect provided the difference between the concerned deformations of intramolecular bonds in polyene and somewhat weaker interionic interactions in CuNCN. Two other force constants get estimates  $K_{cc} = 22750$  K/Å<sup>2</sup> and  $K_{ac} = 2775$  K/Å<sup>2</sup>. With that large difference between the diagonal and off-diagonal force constants we can sometimes assume the matrix  $K^{-1}$  to be diagonal with elements equal to inverse diagonal force constants  $K_{aa}^{-1}$  and  $K_{cc}^{-1}$ .